

# MYBPH, a transcriptional target of TTF-1, inhibits ROCK1, and reduces cell motility and metastasis

Yasuyuki Hosono<sup>1,2</sup>, Tomoya Yamaguchi<sup>1</sup>,  
Eri Mizutani<sup>1</sup>, Kiyoshi Yanagisawa<sup>1,3</sup>,  
Chinatsu Arima<sup>1</sup>, Shuta Tomida<sup>1</sup>,  
Yukako Shimada<sup>1</sup>, Michiyo Hiraoka<sup>1</sup>,  
Seiichi Kato<sup>1</sup>, Kohei Yokoi<sup>2</sup>,  
Motoshi Suzuki<sup>1</sup> and Takashi Takahashi<sup>1,\*</sup>

<sup>1</sup>Division of Molecular Carcinogenesis, Center for Neurological Diseases and Cancer, Nagoya University Graduate School of Medicine, Nagoya, Japan, <sup>2</sup>Department of Thoracic Surgery, Nagoya University Graduate School of Medicine, Nagoya, Japan and <sup>3</sup>Institute for Advanced Research, Nagoya University, Nagoya, Japan

Cell migration driven by actomyosin filament assembly is a critical step in tumour invasion and metastasis. Herein, we report identification of *myosin binding protein H* (MYBPH) as a transcriptional target of *TTF-1* (also known as *NKX2-1* and *TTF1*), a master regulator of lung development that also plays a role as a lineage-survival oncogene in lung adenocarcinoma development. MYBPH inhibited assembly competence-conferring phosphorylation of the myosin regulatory light chain (RLC) as well as activating phosphorylation of LIM domain kinase (LIMK), unexpectedly through its direct physical interaction with Rho kinase 1 (ROCK1) rather than with RLC. Consequently, MYBPH inhibited ROCK1 and negatively regulated actomyosin organization, which in turn reduced single cell motility and increased collective cell migration, resulting in decreased cancer invasion and metastasis. Finally, we also show that MYBPH is epigenetically inactivated by promoter DNA methylation in a fraction of *TTF-1*-positive lung adenocarcinomas, which appears to be in accordance with its deleterious functions in lung adenocarcinoma invasion and metastasis, as well as with the paradoxical association of *TTF-1* expression with favourable prognosis in lung adenocarcinoma patients.

*The EMBO Journal* (2012) 31, 481–493. doi:10.1038/emboj.2011.416; Published online 15 November 2011

Subject Categories: cell & tissue architecture

Keywords: actomyosin; cytoskeleton; lung cancer; ROCK1

## Introduction

Metastasis is thought to be initiated by disruption of cell–cell contact, followed by single cell migration. It is widely accepted that contractile motion of cancer cells is generated by assembly and consecutive contraction of actomyosin

bundles (Lauffenburger and Horwitz, 1996; Friedl and Wolf, 2003; Hall, 2009). Collective cell migration has been shown to result from decreasing actomyosin contractility at the sites of cell–cell contact and plays a role in a range of developmental processes as well as cancer invasion (Christiansen and Rajasekaran, 2006; Hidalgo-Carcedo *et al*, 2011).

Non-muscle myosin II (NM II), a major component of the actomyosin cytoskeleton, comprising two non-muscle myosin heavy chains (NMHCs) and two essential myosin light chains (ELCs), as well as two regulatory light chains (RLCs) (Conti and Adelstein, 2008; Vicente-Manzanares *et al*, 2009). Emerging evidence indicates that NM II members, especially NM IIA, are crucially involved in cancer cell migration, invasion, and metastasis via bivalent binding to actin filaments (Betapudi *et al*, 2006; Huang *et al*, 2009; Medjkane *et al*, 2009). Rho kinase 1 (ROCK1), a downstream effector of RhoA, is a major positive regulator of that process, which is thought to be executed through phosphorylation of RLC and subsequent unfolding of NM IIA into an assembly competent form capable of NM IIA dimer formation. In addition, ROCK1 phosphorylates LIM domain kinase (LIMK) and stabilizes actin filaments through inactivation of the actin-depolymerizing factor cofilin. Another member of the ROCK family, ROCK2, is abundantly and preferentially expressed in non-epithelial tissues such as the brain and muscles, and plays roles in phagocytosis and cell contraction (Etienne-Manneville and Hall, 2002; Riento and Ridley, 2003; Amano *et al*, 2010). However, how actomyosin organization in non-muscle cells is negatively regulated to counterbalance the positive regulatory function of ROCK1 largely remains to be elucidated.

TTF-1 is a lineage-specific transcription factor required for branching morphogenesis and physiological lung functions (Kimura *et al*, 1996). TTF-1 is also involved in pathological conditions of the lung. For example, TTF-1 expression is prominent in lung epithelial cells undergoing regeneration (White *et al*, 2001; Pogach *et al*, 2007). A major fraction of lung adenocarcinomas are also TTF-1 positive, which is suggested to reflect their derivation from the terminal respiratory unit (Yatabe *et al*, 2002; Takeuchi *et al*, 2006). We and others recently identified TTF-1 as a lineage-survival oncogene with focal amplification in lung adenocarcinomas (Kendall *et al*, 2007; Tanaka *et al*, 2007; Weir *et al*, 2007; Kwei *et al*, 2008). However, it is of note that *TTF-1* expression is associated with favourable prognosis in lung adenocarcinoma cases (Anagnostou *et al*, 2009). In the present study, we identified MYBPH as a transcriptional target of TTF-1, which provides a clue for elucidating the molecular mechanism related to how TTF-1 paradoxically inhibits cancer invasion and metastasis.

## Results

### MYBPH is directly transactivated by TTF-1

As an initial step towards a better understanding of transcriptomes regulated by *TTF-1*, microarray analysis was

\*Corresponding author. Division of Molecular Carcinogenesis, Center for Neurological Diseases and Cancer, Nagoya University Graduate School of Medicine, 65 Tsurumai, Showa-ku, Nagoya 466-8550, Japan. Tel.: +81 52 744 2454; Fax: +81 52 744 2457; E-mail: tak@med.nagoya-u.ac.jp

Received: 28 May 2011; accepted: 18 October 2011; published online: 15 November 2011

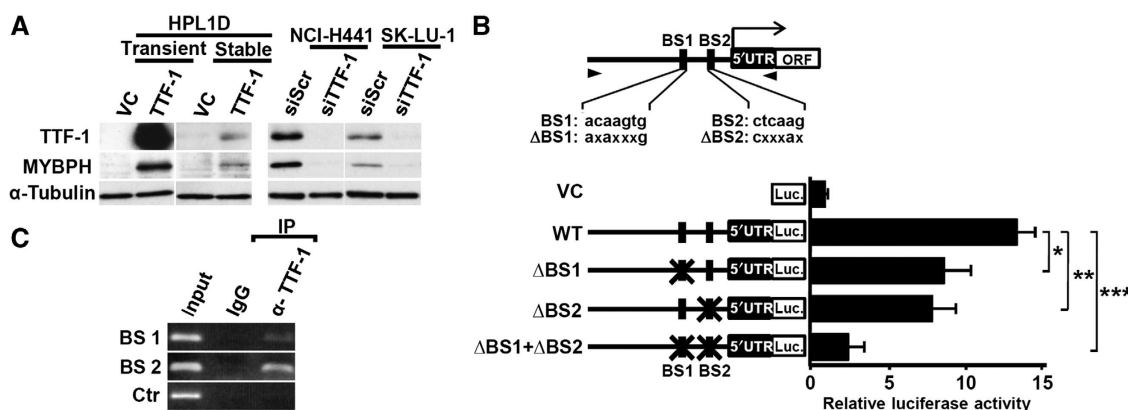


**Figure 1** *MYBPH* is directly transactivated by TTF-1. (A) Western blot analysis showing induction of *MYBPH* in HPL1D cells transiently or stably transfected with TTF-1, as well as reduction by TTF-1 knockdown in NCI-H441 and SK-LU-1 cells. siScr, negative control siRNA; siTTF-1, siRNA against TTF-1. (B) Top panel: schematic diagram of *MYBPH* promoter region, BS1 and BS2, putative NKX2-5 and TTF-1 binding sites, respectively. Arrowheads, locations of primers used to amplify *MYBPH* promoter. Bottom panel: luciferase reporter analysis using HPL1D cells with transient TTF-1-expression. Three independent experiments were performed in triplicate. Bars, mean  $\pm$  s.d.; \* $P < 0.05$ ; \*\* $P < 0.01$ ; \*\*\* $P < 0.005$ . (C) Chromatin immunoprecipitation assay of NCI-H441 cells showing that TTF-1 protein binds to both BS1 and BS2. Figure source data can be found with the Supplementary data.

performed using an immortalized peripheral lung epithelial cell line, HPL1D (Masuda *et al*, 1997), which was transiently transfected with *TTF-1*. We consequently identified *MYBPH* as the most highly upregulated gene (Supplementary Figure S1) and confirmed its upregulation at the protein level by western blot analysis (Figure 1A). A dual-luciferase assay also revealed *TTF-1*-mediated transcriptional activation of *MYBPH* (Figure 1B; Supplementary Figure S2A), while a chromatin immunoprecipitation (ChIP) assay of NCI-H441 cells clearly demonstrated specific binding of TTF-1 with both potential TTF-1 binding sites in the *MYBPH* promoter (Figure 1C).

### ***MYBPH* expression is inactivated by the promoter CpG methylation**

TTF-1 was invariably present in lung adenocarcinoma cell lines expressing *MYBPH* at readily detectable levels (Figure 2A), while a significant correlation between TTF-1 and *MYBPH* expression was also observed in the analysis of our previous microarray data set of 90 lung adenocarcinoma cases ( $P = 0.0051$ ; Figure 2B; Takeuchi *et al*, 2006). Interestingly, however, we noted that a considerable fraction of lung adenocarcinomas both *in vitro* and *in vivo* expressed low levels of *MYBPH* despite high *TTF-1* expression. Therefore, we evaluated whether aberrant DNA methylation of the *MYBPH* promoter was involved in silencing of *MYBPH*. Treatment with a DNA demethylating agent, 5-Aza-dC, significantly induced *MYBPH* in NCI-H358 and A427 cells (Figure 2C), while bisulphite sequencing analysis revealed clear distinctions in terms of dense DNA methylation surrounding the genuine TTF-1 binding site (BS2; Li *et al*, 1998), but not that for the TTF-1 homologue, NKX2-5 (BS1; Chen and Schwartz, 1995), in NCI-H358 and A427 cells (Figure 2D; Supplementary Figure S2B). Methylation-specific PCR (MSP) analysis using DNA from laser microdissected specimens further confirmed the presence of aberrant DNA methylation specifically in *MYBPH*<sup>-</sup>/*TTF-1*<sup>+</sup> lung adenocarcinoma tissues *in vivo* (Figure 2E). The present findings thus indicate that *MYBPH* is a direct transcriptional target of *TTF-1*, which is inactivated by promoter DNA methylation in a considerable fraction of lung adenocarcinomas.

### ***MYBPH* reduces cell motility, invasion, and metastasis**

NM II is a major component of the actomyosin cytoskeleton in non-muscle cells and crucially involved in cell migration (Betapudi *et al*, 2006; Conti and Adelstein, 2008; Huang *et al*, 2009; Medjkane *et al*, 2009; Vicente-Manzanares *et al*, 2009). The presence of inactivating promoter DNA methylation led us to speculate that *TTF-1*-induced *MYBPH* might play a negative regulatory role in cell motility. Indeed, we found that treatment with small interfering RNA (siRNA) against *MYBPH* (siMYBPH) markedly increased the motility of NCI-H441 cells. Conversely, overexpression of *MYBPH* reduced Madin-Darby canine kidney (MDCK) cell motility (Figure 3A; Supplementary Figure S3), while that negative effect was cancelled by simultaneous treatment with siMYBPH (Supplementary Figure S4). Similarly, acquisition of the motile phenotype in siMYBPH-treated NCI-H441 cells was clearly demonstrated by results of a scratch assay (Figure 3B) as well as those of a Matrigel invasion assay (Figure 3C), with opposite effects observed in *MYBPH*-overexpressing MDCK cells. Next, we employed a three-dimensional Matrigel invasion assay and found that *MYBPH*-overexpressing MDCK cells invaded over a shorter distance and in a more collective manner than the control cells (Figure 3D). Neither siMYBPH treatment of NCI-H441 cells nor forced *MYBPH* overexpression in MDCK cells had an effect on cell growth (Supplementary Figure S5). We also noted that overexpression of TTF-1 reduced cell motility in HPL1D cells, which was significantly reverted by siMYBPH treatment (Figure 3E), supporting the notion that TTF-1-induced *MYBPH* negatively affects cell motility.

We also evaluated the effects of *MYBPH* expression on metastasis using a highly metastatic *MYBPH*-negative lung cancer cell line, NCI-H460-LNM35 (Kozaki *et al*, 2000). Stable transfectants expressing *MYBPH* at a level comparable to that in lung adenocarcinoma cell lines (Figure 4A) exhibited significantly reduced lung metastasis (Figure 4B and C), without affecting primary tumour growth (Supplementary Figure S6). Conversely, siMYBPH-treated NCI-H441 cells exhibited increased experimental lung metastasis (Figure 4D and E). In line with the present experimental findings, it was noted that decreased *MYBPH* expression was significantly

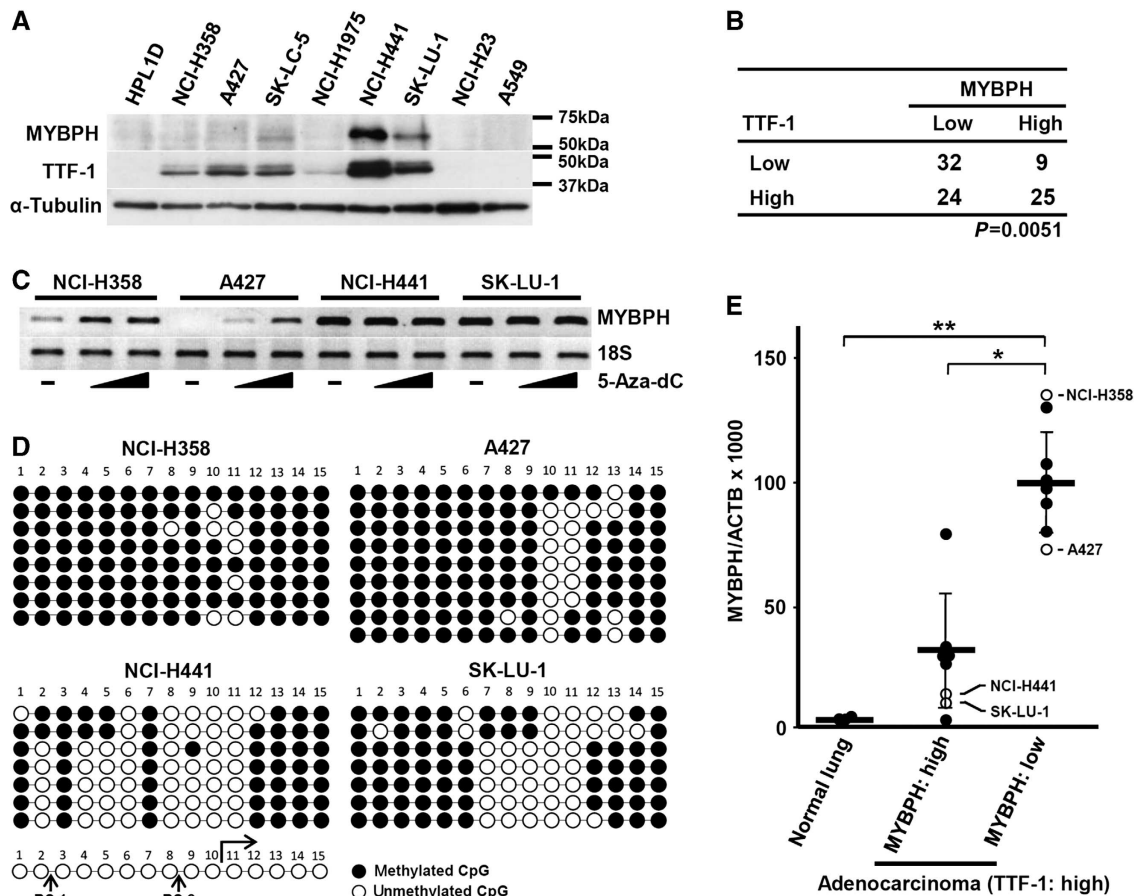


**Figure 2** MYBPH expression is inactivated by the promoter CpG methylation. (A) Western blot analysis of MYBPH and TTF-1 in lung adenocarcinoma cell lines. (B) Correlation between *TTF-1* and *MYBPH* expressions in 90 lung adenocarcinoma specimens. Cases were classified into those above or below the average level of expression. (C) Semiquantitative RT-PCR analysis of four cell lines showing *MYBPH* induction in TTF-1<sup>+</sup>/MYBPH<sup>-</sup>NCI-H358 and A427 cells after treatment with 5-Aza-dC. 18S served as a loading control. (D) Bisulphite sequencing analysis showing dense DNA methylation around BS2 in TTF-1<sup>+</sup>/MYBPH<sup>-</sup>NCI-H358 and A427 cells. (E) Methylation-specific PCR analysis of the eighth CpG site in (D) using DNA from laser microdissected specimens and representative cell lines, which revealed aberrant DNA methylation in TTF-1<sup>+</sup>/MYBPH<sup>-</sup> lung adenocarcinoma tissues and cell lines. Six cases each of MYBPH-positive and -negative lung adenocarcinomas with abundant TTF-1 expression, along with three normal lung tissues were analysed. Solid circles, clinical samples; open circles, cell lines; bars, mean  $\pm$  s.d.; \* $P < 0.001$ ; \*\* $P < 0.0001$ . Figure source data can be found with the Supplementary data.

associated with more apparent invasiveness in surgical specimens obtained from the 90 human lung adenocarcinoma cases (Figure 4F).

### MYBPH affects actomyosin organization and cell morphology

We also found that siMYBPH treatment markedly altered the shape of the cells, as they showed a rounded morphology or occasionally bleb-like structures characterized by the appearance of peripheral actomyosin bundles, with clear colocalization of NMHC IIA with the peripheral actin bundles (Figure 5A; Supplementary Figure S7, left). Conversely, overexpression of MYBPH disrupted actomyosin organization as well as the normal morphology in MDCK cells (Figure 5B; Supplementary Figure S7, right). Taken together, these findings strongly support the notion that MYBPH is involved in the regulation of cell shape, motility, invasion, and metastasis.

### MYBPH inhibits phosphorylation of RLC through interaction with ROCK1

Our findings strongly suggested that MYBPH is involved in actin organization. We, therefore, analysed changes in the

proportion of triton-insoluble F-actin (TIF), a crosslinked meshwork of actin filaments that includes stress fibers (Watts and Howard, 1992), in relation to the level of MYBPH expression. We observed that siMYBPH-treated NCI-H441 cells contained a larger proportion of TIF pools than those treated with the siRNA control. In contrast, MYBPH-introduced MDCK cells contained fewer TIF pools than the control cells (Figure 6A).

Phosphorylation of RLC unfolds assembly incompetent NM IIA into assembly competent NM IIA, which is a prerequisite for its assembly and subsequent actomyosin reorganization (Conti and Adelstein, 2008; Vicente-Manzanares *et al*, 2009). In this connection, we found that NCI-H441 knocked down for MYBPH exhibited increased RLC phosphorylation, whereas introduction of MYBPH reduced the RLC phosphorylation level in MDCK cells (Figure 6B). This finding prompted us to investigate whether MYBPH is involved in the regulation of ROCK-mediated phosphorylation of RLC, since ROCK1 and 2 have been shown to play a central role in the regulation of RLC phosphorylation as downstream effectors of RhoA (Conti and Adelstein, 2008; Vicente-Manzanares *et al*, 2009). *In-vitro* protein-protein binding

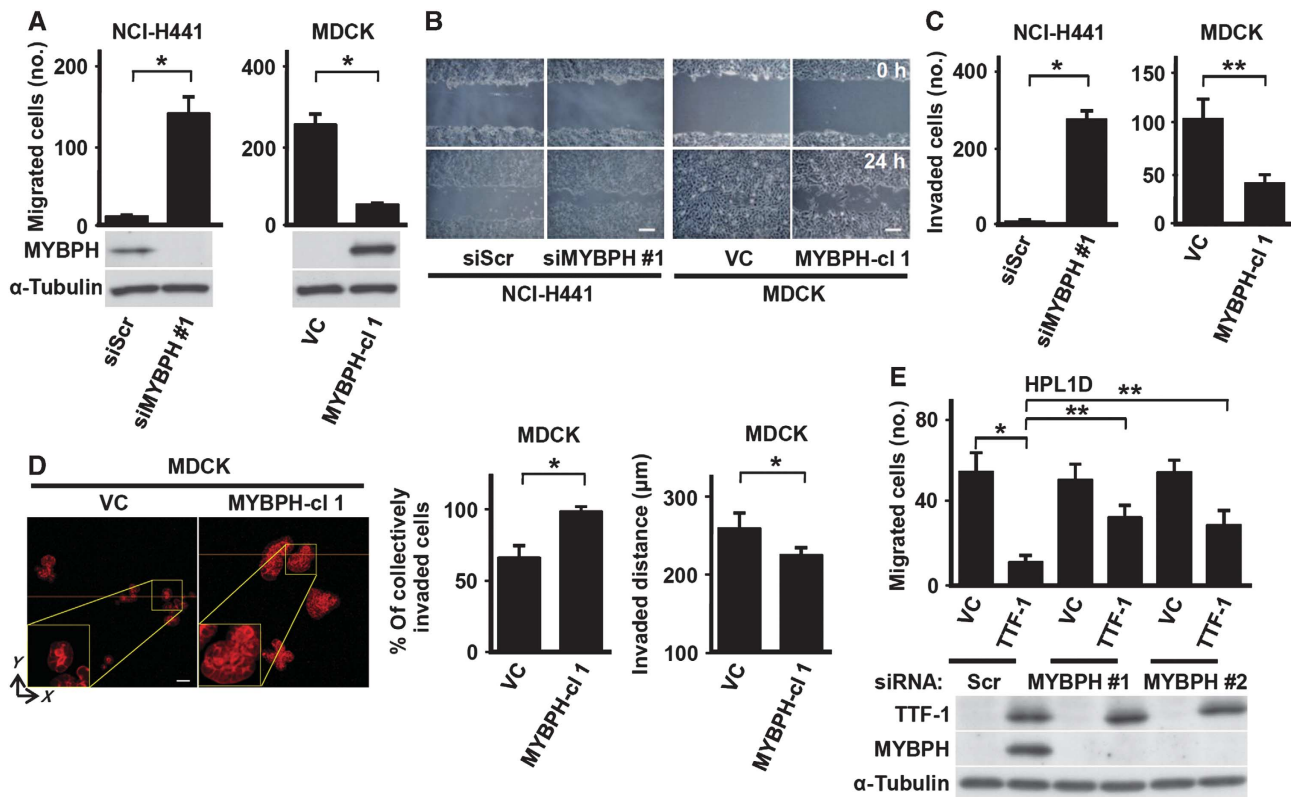


**Figure 3** MYBPH reduces cell motility and invasion *in vitro*, and increases collective cell migration. (A) Motility assay showing increased *in-vitro* motility by MYBPH knockdown in NCI-H441 cells as well as reduced motility in stable MYBPH transfectant of MDCK cells. Three independent experiments were performed in triplicate. siMYBPH, siRNA against MYBPH; MYBPH-cl 1, MYBPH-transfected clone; bars, mean  $\pm$  s.d.; \* $P$ <0.01. Results of corresponding western blot analysis of MYBPH are shown below. (B) Scratch assay showing increased *in-vitro* motility by MYBPH knockdown in NCI-H441 cells as well as reduced motility in stable MYBPH transfectant of MDCK cells. Photographs were taken at 24 h after scratch injury. Bars indicate 200  $\mu$ m. (C) Matrigel invasion assay showing increased *in-vitro* invasion by MYBPH knockdown in NCI-H441 cells as well as reduced invasion in stable MYBPH transfectant of MDCK cells. Three independent experiments were performed in triplicate. Bars, mean  $\pm$  s.d.; \* $P$ <0.001; \*\* $P$ <0.01. (D) Three-dimensional Matrigel invasion assay showing collective cell migration and decreased *in-vitro* invasion in stable MYBPH transfectant of MDCK cells. The proportions of cells with collective invasion were evaluated as described in Materials and methods. Data shown represent four independent experiments each counting > 100 cells. White bars indicate 50  $\mu$ m. Bars, mean  $\pm$  s.d.; \* $P$ <0.001. (E) Motility assay findings showing reduced *in-vitro* motility in stable TTF-1 transfectants of HPL1D cells, which was cancelled by treatment with siMYBPH. Three independent experiments were performed in triplicate. Bars, mean  $\pm$  s.d.; \* $P$ <0.01; \*\* $P$ <0.05. The results of corresponding western blot analyses of TTF-1 and MYBPH are shown below. Figure source data can be found with the Supplementary data.

assays were performed to examine whether MYBPH directly interacts with RLC and/or ROCK1 and 2, using a purified His-tagged MYBPH protein with either purified GST-tagged ROCK1, ROCK2, or RLC proteins. Consequently, a direct interaction of MYBPH specifically with ROCK1, but not with RLC, was unexpectedly revealed (Figure 6C). *In-vitro* ROCK kinase assays using purified ROCK1, ROCK2, and RLC proteins in the presence or absence of purified MYBPH protein demonstrated inhibition of ROCK1-mediated RLC phosphorylation by inclusion of MYBPH in the reaction mixture, whereas the presence of MYBPH had no effects on ROCK2-mediated RLC phosphorylation *in vitro*, consistent with the *in-vitro* binding assay results (Figure 6D; Supplementary Figure S8). We also noted that MYBPH was not phosphorylated by either ROCK1 or ROCK2 (Supplementary Figure S8). Immunoprecipitation–western blot (IP–WB) analysis also showed an association of MYBPH with ROCK1 in MYBPH-overexpressing MDCK and NCI-H441 cells, respectively (Figure 6E; Supplementary Figure S9). Overexpression of MYBPH reduced the interaction between ROCK1 and RLC in MDCK, whereas siMYBPH treatment increased their interaction in NCI-H441 cells (Figure 6F). In contrast, the interaction

between RhoA and ROCK1 was not affected by MYBPH (Supplementary Figure S10), which appears to be consistent with the interaction of MYBPH with purified GST-tagged ROCK1 protein lacking a RhoA-binding domain near the C-terminus. In addition, IP–WB analysis showed lack of interactions of MYBPH with various RLC kinases (Supplementary Figure S11), including myosin light chain kinase (MLCK), myotonic dystrophy kinase-related CDC42 binding protein kinase alpha and beta (MRCK $\alpha$  and  $\beta$ ), citron, and Zipper interacting protein kinase (ZIPK) (Matsumura, 2005).

Further analysis using various deletion mutants of MYBPH showed that the fibronectin type III domain of MYBPH was required for MYBPH binding to ROCK1 (Figure 7A; Supplementary Figure S12). Consistently, a deletion mutant devoid of the fibronectin type III domain did not elicit MYBPH overexpression-induced alterations in cell morphology and actomyosin bundle formation or decreased cell motility in MDCK cells (Figure 7B; Supplementary Figure S13). We also found that MYBPH affects the phosphorylation state of LIMK and cofilin (Figure 7C), which are known to participate in the cascade downstream of ROCK1, thus regulating actin polymerization (Maekawa *et al*, 1999; Yoshioka



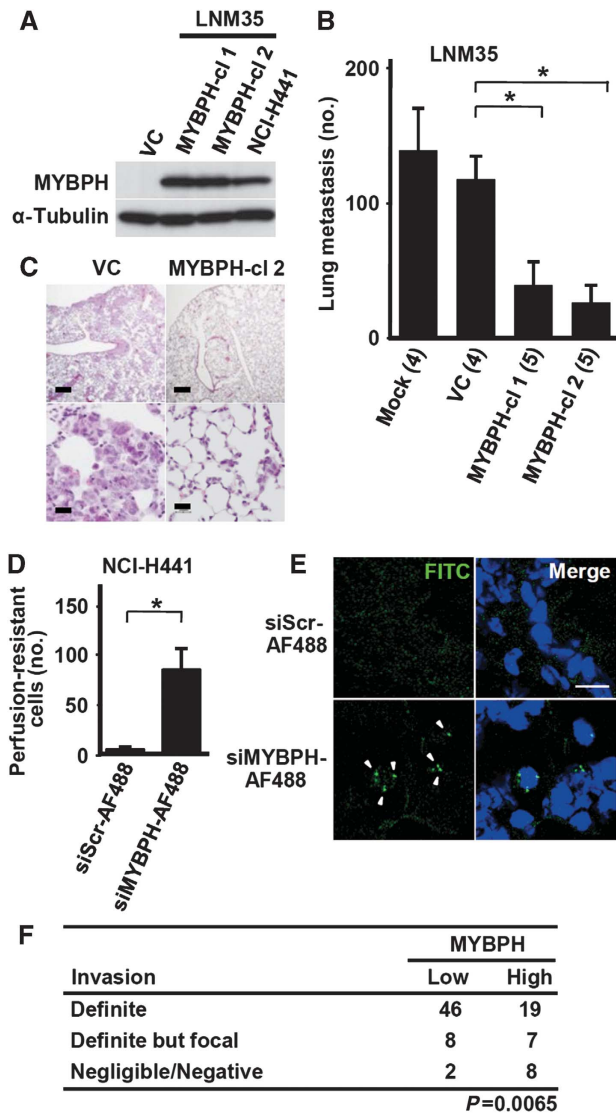


**Figure 4** MYBPH reduces invasion and metastasis *in vivo*. (A) Western blot analysis showing expression levels of MYBPH in stable transfectants of NCI-H460-LNM35 (LNM35-MYBPH-cl 1 and cl 2) expressing MYBPH at a level comparable to that in NCI-H441. (B) Decreased lung metastasis in stable MYBPH transfectants of LNM35. Forty days after subcutaneous inoculation, lung metastases were counted. Bars, mean  $\pm$  s.d.; \* $P < 0.01$ . Numbers in parentheses indicate inoculated mice. (C) Representative haematoxylin and eosin-stained images of lung metastases. Bars indicate 200  $\mu$ m in upper and 20  $\mu$ m in lower panels. (D) Experimental metastasis assay of NCI-H441 cells knocked down for MYBPH with Alexa Fluor 488-conjugated siMYBPH #1 (siMYBPH #1-AF488) (five mice per treatment). Bars, mean  $\pm$  s.d.; \* $P < 0.001$ . (E) Representative fluorescence images of perfusion-resistant cells. Cells were also stained with DAPI (blue). Bars indicate 10  $\mu$ m. (F) Relationships between MYBPH expression and invasion status in our previously reported microarray data set of human lung adenocarcinomas. Cases were classified into those above and below the average level of expression. Figure source data can be found with the Supplementary data.

*et al*, 2003). Consistent with the present findings, increased motility, RLC phosphorylation, and organization of peripheral actomyosin bundles induced by MYBPH knockdown in NCI-H441 cells were significantly, though not completely, counteracted by simultaneous treatment with the ROCK-specific inhibitor Y-27632 (Figure 7D; Supplementary Figure S14). It was also found that increased cell motility

and RLC phosphorylation induced by siMYBPH treatment were counteracted by simultaneous treatment with siROCK1, but not with siROCK2 (Figure 7E). Thus, it was demonstrated that MYBPH binds to ROCK1 but not to RLC, leading to inhibition of ROCK1-mediated regulation of actomyosin organization including assembly competence-conferring RLC phosphorylation and activation of the LIMK-cofilin pathway.

### MYBPH increases cell-cell contact and collective cell migration

A decrease in ROCK-driven actomyosin contractility enhances cell-cell contact and collective cancer cell invasion (Sahai and Marshall, 2002; Hidalgo-Carcedo *et al*, 2011). Along this line, NCI-H441 cells knocked down for MYBPH migrated mostly as single cells in a three-dimensional invasion assay, which was reverted by simultaneous treatment with Y-27632 (Figure 8A). This siMYBPH-mediated increase in single cell migration was markedly counteracted by simultaneous treatment with siROCK1 (Figure 8B). While one of the hallmarks characterizing collective cell migration is preservation of the integrity of cell-cell contact during movement (Friedl and Gilmour, 2009), MYBPH knockdown markedly decreased cell-cell contact in NCI-H441 cells, as shown in our aggregation assay. This effect was clearly counteracted by a simultaneous treatment with Y-27632 (Figure 8C). Conversely, overexpression of MYBPH reduced MDCK cell aggregation (Figure 8D). Formation of adherence junctions positively regulate cell-cell contacts in epithelial cells (Friedl and Wolf, 2010). Our aggregation assay findings showed that siMYBPH-treated NCI-H441 cells exhibited a readily detectable decrease in E-cadherin staining intensity on the cell surface, which was considerably counteracted by simultaneous treatment with Y-27632 (Figure 8E). Conversely, overexpression of MYBPH increased E-cadherin intensity in MDCK cells similarly examined by an aggregation assay (Supplementary Figure S15). Interestingly, western blot analysis demonstrated similar levels of E-cadherin expression irrespective of MYBPH state. Taken together, the present findings indicate that TTF-1-inducible MYBPH inhibits ROCK1 through direct interaction, which in turn negatively regulates actomyosin organization, leading to decreased cell motility, invasion, and metastasis (Figure 9).

## Discussion

The present findings indicate that MYBPH, which we identified here as a direct transcriptional target of TTF-1, plays multiple roles in negative regulation of actomyosin organization. Among the various myosin binding proteins, a cardiac isoform of MYBPC (*cMYBPC*) has been the focus of intense research activities, because of its direct involvement in cardiovascular diseases such as familial hypertrophic cardiomyopathy (Bonne *et al*, 1995; Watkins *et al*, 1995; Richard *et al*, 2003). While MYBPH and *cMYBPC* possess significant homology at their carboxyl termini, MYBPH lacks a region homologous to the amino terminal half of *cMYBPC*, which is required for inhibition of myosin functions. To date, very little is known about the functions of MYBPH, even in regard to its interaction with muscle myosin (Yamamoto, 1988; Welikson and Fischman, 2002), with virtually nothing reported regarding its roles in non-muscle cells.

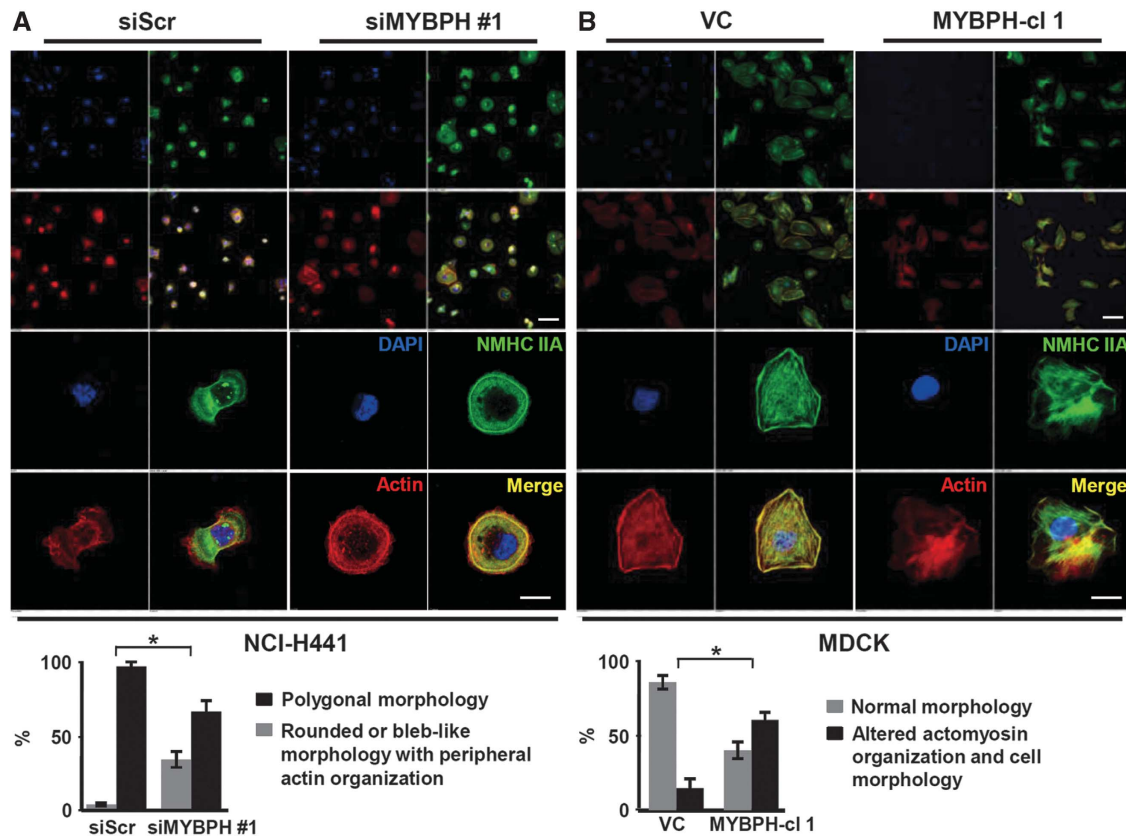


**Figure 5** MYBPH affects actomyosin organization and cell morphology. (A) Top panels: immunofluorescence staining for DAPI (blue), actin (red), and NMHC IIA (green) in NCI-H441 cells treated with siScr or siMYBPH. Bars indicate 100  $\mu$ m in top and 10  $\mu$ m in bottom panels. Bottom panel: proportions of cells according to morphology. Data shown represent three independent experiments each counting > 100 cells. Bars, mean  $\pm$  s.d.; \* $P$ <0.001. Results with an additional siMYBPH are also shown in the left panels of Supplementary Figure S7. (B) Top panels: immunofluorescence staining for DAPI (blue), actin (red), and NMHC IIA (green) in MDCK cells stably transfected with empty or MYBPH-expressing vectors. Bars indicate 100  $\mu$ m in top and 10  $\mu$ m in bottom panels. Bottom panel: proportions of cells according to morphology, which were determined as shown in (A). Bars, mean  $\pm$  s.d.; \* $P$ <0.001. Results obtained with an additional independent clone are shown in the right panels of Supplementary Figure S7.

In this study, we found that MYBPH inhibits assembly competence-conferring RLC phosphorylation as well as activating phosphorylation of LIMK. MYBPH unexpectedly executes such inhibitory activities by direct physical interaction with ROCK1 rather than with RLC, which results in inhibition of ROCK1 kinase activity. ROCK1 is a downstream effector of RhoA that is crucially involved in cell morphogenesis and motility, as well as in cancer progression (Itoh *et al*, 1999; Sahai and Marshall, 2003; Wilkinson *et al*, 2005; Wong *et al*, 2008). To date, however, very few examples have been reported as negative regulators of ROCK1. While RhoE has been shown to inhibit ROCK1 by competing with RhoA for ROCK1 (Riento *et al*, 2003), MYBPH directly binds to and interferes with ROCK1, which in turn inhibits RLC phosphorylation. Our findings thus add MYBPH to the small list of negative ROCK1 regulators, suggesting a complex nature of the negative regulatory mechanisms of ROCK1.

It is interesting that marked distinctions were observed in terms of specificities of the binding and inhibitory capabilities of MYBPH towards ROCK1 and ROCK2. Along line, it is important to note that RhoE binds to ROCK1 but not to ROCK2 and inhibits its function, resulting in loss of stress fiber formation (Riento *et al*, 2003). It was also reported that siRNA-mediated ROCK1 knockdown results in loss of stress fibers, in contrast to lack of such effects in cells knocked

down for ROCK2 (Yoneda *et al*, 2005). Together, these findings indicate that ROCK1 plays a major role in stress fiber formation and are in line with the present findings of actomyosin regulation by MYBPH through ROCK1 inhibition.

Considering that ROCK1 also mediates regulatory phosphorylation of various other molecules, such as endothelial nitric oxide synthase (eNOS) and collapsin response mediator protein 2 (CRMP2), and is involved in a wide range of disease states including vasospasms, pulmonary hypertension, and nerve injury (Etienne-Manneville and Hall, 2002; Riento and Ridley, 2003), it would be interesting to investigate whether MYBPH might be involved in such disease states as a regulator of ROCK1. In addition, given that collective cell migration plays an important role in various physiological settings including morphogenesis, tissue regeneration, and repair of wounded epithelial tissues (Kimura *et al*, 1996; White *et al*, 2001; Pogach *et al*, 2007), it is of note that changes in MYBPH expression alter actomyosin organization, and consequently affect collective cell migration, especially when considering that TTF-1 is a master regulatory transcription factor involved in peripheral lung development (Kimura *et al*, 1996; Yatabe *et al*, 2002) and that type II pneumocyte hyperplasia, a reconstitution process of the alveolar lining, is associated with increased TTF-1 expression (White *et al*, 2001; Pogach *et al*, 2007).

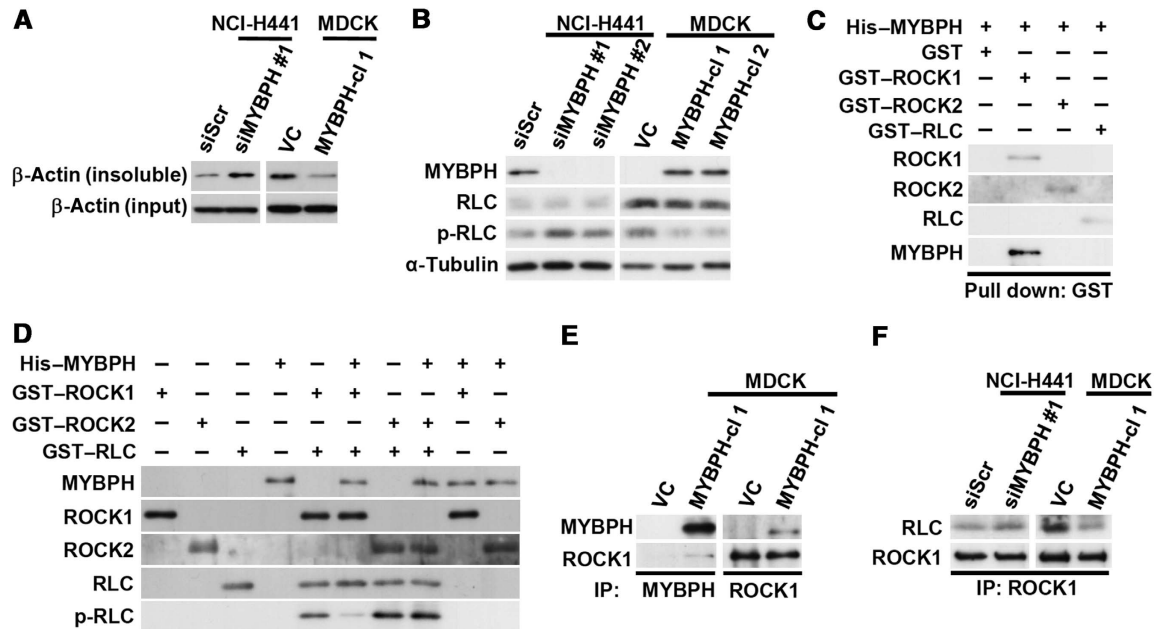


**Figure 6** MYBPH inhibits phosphorylation of RLC through interaction with ROCK 1. (A) Actin assembly assay showing an increase in triton-insoluble unassembled F-actin (TIF) in siMYBPH-treated NCI-H441 cells as well as opposite effects by MYBPH introduction in MDCK cells. (B) Western blot analysis showing induction of RLC phosphorylation by MYBPH knockdown in NCI-H441 cells as well as reduction in MYBPH transfectants of MDCK cells. p-RLC, phospho-RLC (T18/S19). (C) *In-vitro* protein-protein binding assay results showing interaction of purified MYBPH with ROCK1, but not with ROCK2 or RLC. (D) *In-vitro* ROCK kinase assay using purified RLC protein as a substrate, showing inhibition of ROCK1-mediated RLC phosphorylation by MYBPH. (E) Immunoprecipitation-western blot (IP-WB) analysis showing co-immunoprecipitation of MYBPH with ROCK1 in MDCK cells expressing exogenous MYBPH. (F) IP-WB analysis showing increased interaction between ROCK1 and RLC by siMYBPH treatment in NCI-H441 cells. Conversely, their reduced interaction was seen in MDCK cells stably transfected with MYBPH. Figure source data can be found with the Supplementary data.

Our results clearly demonstrate that MYBPH negatively regulates cell motility, invasion, and metastasis. Thus, it is quite conceivable that MYBPH induction by TTF-1 is deleterious for lung adenocarcinoma progression, which is thereby inactivated by promoter DNA methylation in a fraction of TTF-1-positive lung adenocarcinomas. This finding in turn resolves a question arising from previous observations that a high level of TTF-1 expression, which we and others have identified as a lineage-survival oncogene in lung adenocarcinoma (Kendall *et al*, 2007; Tanaka *et al*, 2007; Weir *et al*, 2007; Kwei *et al*, 2008), is paradoxically associated with favourable prognosis (Anagnostou *et al*, 2009). We note that during the preparation of this manuscript, Jacks and colleagues reported that TTF-1 downregulation was associated with tumour progression and acquisition of metastatic ability, in association with derepression of HMGA2 in a lung adenocarcinoma model of mutant K-ras/p53 conditional knockout (Winslow *et al*, 2011). Our findings further indicate that MYBPH plays a crucial role as a positively regulated downstream effector of TTF-1, with capabilities for inhibiting cancer cell motility, invasion, and metastasis. Thus, both transcriptional activation and repression by TTF-1 appear to be engaged in conferring a less aggressive phenotype, despite its opposing role as a lineage-survival oncogene in TTF-1-positive lung adenocarcinomas (Kendall *et al*, 2007; Tanaka *et al*, 2007; Weir *et al*, 2007; Kwei *et al*, 2008).

## Materials and methods

### Cell lines

The derivation, characteristics, and culture conditions of the human lung adenocarcinoma cell lines utilized, and the immortalized

human lung epithelial cell line HPL1D as well as the highly metastatic NCI-H460-LNM35 (LNM35) lung cancer cell line were previously reported (Masuda *et al*, 1997; Kozaki *et al*, 2000; Tanaka *et al*, 2007). An MDCK cell line was purchased from RIKEN Cell Bank and maintained in Dulbecco's Modified Eagle's Medium containing 10% fetal bovine serum.

### Antibodies, reagents, and oligonucleotide primers

The anti-TTF-1 antibody for western blot analysis was purchased from DAKO; anti-TTF-1 for the ChIP assay from Thermo; anti-MYBPH from Abnova; anti-E-cadherin from BD Transduction Laboratories; anti-GST and anti-His from MBL; anti-NMHC IIA, anti-MLCK, anti-β-actin, and anti-α-tubulin from Sigma-Aldrich; anti-ROCK1, anti-ROCK2, anti-RLC, anti-phospho-RLC (T18/S19), anti-cofilin, anti-phospho-cofilin (S3), anti-phospho-LIMK1 (T508)/LIMK2 (T505), anti-mouse IgG, and anti-rabbit IgG from Cell Signalling Technology; anti-Citron from Novus; anti-RhoA, anti-MRCK-α, and anti-MRCK-β from Santa Cruz; and anti-ZIPK from Calbiochem. ROCK-specific inhibitor Y-27632 was also purchased from Calbiochem. The sequences of the oligonucleotide primers used for PCR and sequencing are provided in Supplementary Table S1.

### DNA constructs

The expression construct of full-length human TTF-1 (pCMV-puro-TTF-1) was previously described (Tanaka *et al*, 2007). Full-length human MYBPH cDNA (OpenBio) was inserted into a pCMV-puro vector and the entire open reading frame of the resultant construct (pCMVpuro-MYBPH) was thoroughly sequenced. Transfection was performed using FuGENE6 (Roche), followed by puromycin selection.

### Microarray data

RNA was extracted from HPL1D cells transiently transfected with TTF-1 or an empty vector followed by puromycin selection for 3 days, and analysed in duplicate (GSE26721), using a low RNA fluorescent linear amplification kit and 44K whole human genome microarrays (Agilent Technologies), essentially as described previously (Tomida *et al*, 2009). Our previously obtained micro-

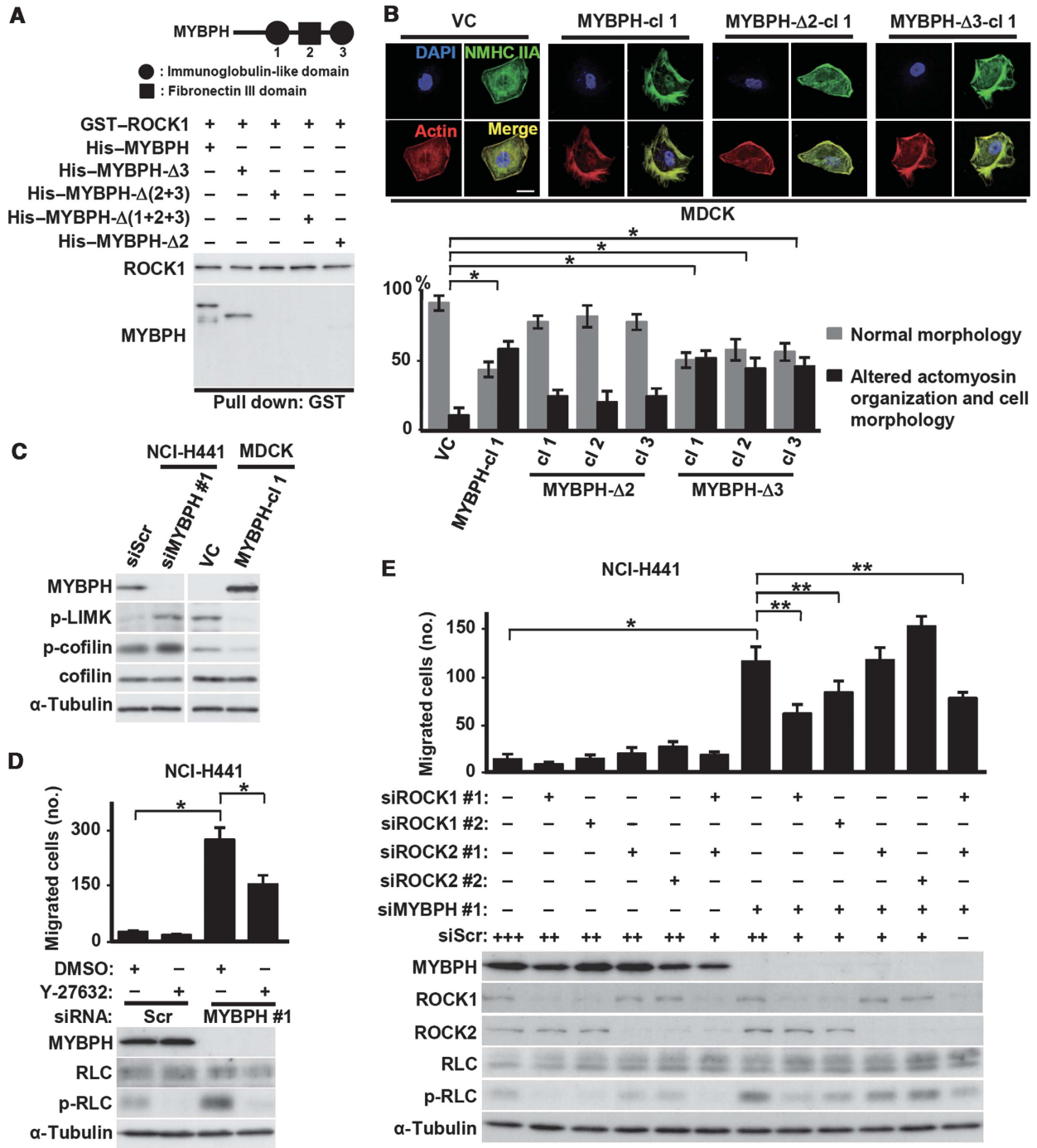


**Figure 7** MYBPH knockdown-induced effects on actin bundle formation, cell motility and RLC phosphorylation are alleviated through ROCK1 binding and inhibition. (A) Top panel: schematic representation of domain organization of MYBPH. Bottom panel: *in vitro* protein-protein binding assay showing requirement of a fibronectin type III domain of MYBPH for its binding with ROCK1. Western blot analysis of His-tagged MYBPH-wt, -Δ3, -Δ(2+3), -Δ(1+2+3), and -Δ2 proteins are shown in Supplementary Figure S12. (B) Top panels: immunofluorescence staining for DAPI (blue), actin (red), and NMHC IIA (green) in MDCK cells stably introduced with an empty vector (VC), or MYBPH expression constructs of wild-type or deletion mutants lacking either fibronectin type III (MYBPH-Δ2) or immunoglobulin-like domains. Bars indicate 10 μm. Bottom panel: proportions of cells according to morphology, which were determined as shown in Figure 5A. Bars, mean ± s.d.; \**P* < 0.001. (C) Western blot analysis showing induction of LIMK and cofilin phosphorylation by MYBPH knockdown in NCI-H441 cells as well as reduction in MYBPH transfectant of MDCK cells. p-LIMK, phospho-LIMK1 (T508)/LIMK2 (T505); p-cofilin, phospho-cofilin (S3). (D) Top panel: partial cancellation of the MYBPH knockdown-induced motility by a simultaneous treatment with a ROCK-specific inhibitor Y-27632 in NCI-H441 cells. Bars, mean ± s.d.; \**P* < 0.01. Bottom panel: representative western blot images for RLC phosphorylation. (E) Top panel: partial cancellation of MYBPH knockdown-induced motility by simultaneous treatment with siRNAs against ROCK1 in NCI-H441 cells. Bars, mean ± s.d.; \**P* < 0.01; \*\**P* < 0.05. Bottom panel: representative western blot images for RLC phosphorylation. siRNA concentrations: +, 40 nM; ++, 80 nM; +++, 120 nM. Figure source data can be found with the Supplementary data.

array data of 90 lung adenocarcinoma cases (Takeuchi *et al*, 2006; GSE11969) were used to analyse the association of *MYBPH* expression with *TTF-1* expression as well as with various clinical parameters.

#### siRNA treatment

siRNA duplexes targeting TTF-1 (siTTF-1) and MYBPH (siMYBPH #1 and #2 as well as siMYBPH-AF488, Alexa Fluor 488-conjugated siMYBPH #1) and a negative control (siScr) were obtained from



Sigma Genosys, while siRNA duplexes targeting ROCK1 (siROCK1 #1 and #2) and ROCK2 (#1 and #2) from Invitrogen. Transfection of each siRNA at 40 nM was performed using Lipofectamine RNAi-MAX (Invitrogen). Cells were harvested at 48 h after transfection for each assay. The sequences of the siRNAs are provided in Supplementary Table S1.

#### Western blot analysis

Western blot analysis was performed according to standard procedures using Immobilon-P filters (Millipore) and an Enhanced Chemiluminescence system (GE Healthcare). NCI-H441 cells were treated with Y-27632 (5  $\mu$ M) for 15 min before.

#### IP-WB analysis

Cells ( $2 \times 10^7$ ) were lysed with modified RIPA buffer containing protease inhibitor cocktail Tablets (Roche) and incubated with each antibody overnight at 4°C, followed by addition of protein G Sepharose (GE Healthcare) and subsequent incubation for an additional 1 h. The immunoprecipitates were analysed by western blot analysis.

#### Dual-luciferase reporter assay

An MYBPH luciferase reporter construct was generated using a pGL4 basic reporter vector (Promega) and a PCR-amplified 1.0-kb genomic fragment from the MYBPH promoter region. Mutant vectors carrying deletions at the predicted binding sites for *TTF-1* and *NKX2-5* were constructed using a QuikChange site-directed mutagenesis kit (Stratagene). HPL1D cells ( $3.0 \times 10^5$ ) transiently expressing *TTF-1* were transfected with each pGL4 vector (1.8  $\mu$ g) together with a pRLTK vector (0.2  $\mu$ g), then the cell lysates were collected after 48 h. Luciferase reporter activities were determined using a Dual-Luciferase Reporter Assay System (Promega). Firefly luciferase activity was normalized with that of Renilla luciferase.

#### ChIP assay

NCI-H441 cells ( $1.0 \times 10^8$ ) were harvested after crosslinking with 1% formaldehyde. Chromatin was sheared by sonication to an average length of 500–600 bp, followed by immunoprecipitation with a TTF-1-specific antibody. After reversal of crosslinking, immunoprecipitated chromatin was subjected to PCR using primers for the predicted binding sites of *TTF-1* and *NKX2-5* as well as those for an unrelated genomic region as a negative control.

#### Treatment with 5-aza-2'-deoxycytidine

Cells ( $1.0$ – $1.5 \times 10^5$ ) were incubated with 1 or 2  $\mu$ M of 5-aza-2'-deoxycytidine (5-Aza-dC; Sigma) for 5 days. Media were changed every 24 h. Semiquantitative PCR was performed using primers for amplification of the coding region of MYBPH.

#### Bisulphite sequencing analysis

Bisulphite conversion of genomic DNA was performed using MethylEasy Xceed™ (Human Genetic Signatures), according to the manufacturer's instructions. The MYBPH promoter region was amplified using nested primers and the resultant PCR products were cloned into pGEM-T easy vectors (Promega), followed by sequencing of randomly selected clones.

#### Laser microdissection and MSP

Cancer cells were microdissected from 20  $\mu$ m thick frozen sections using a Leica LMD 7000 Laser Micro-dissection system (Leica Microsystems). Bisulphite-modified DNA was used as a template for SYBR Green (Applied Biosystems)-based real-time PCR, with primers designed for specific detection of methylated DNA at a CpG (#8) close to the TTF-1-binding consensus sequence of the MYBPH promoter and a promoter region without CpG sites of the reference gene, *ACTB*. The methylation level in the MYBPH promoter was determined as the ratio of methylation-specific PCR-amplified MYBPH gene to ACTB reference gene, and then multiplied by 1000 for easier tabulation.

#### In-vitro motility, invasion, scratch, and MTT assays

*In-vitro* motility and invasion assays were essentially performed as previously described (Kozaki *et al*, 2000). For each assay,  $1 \times 10^5$  MDCK cells,  $1.5 \times 10^5$  NCI-H441, and HPL1D cells were added to the upper chambers, then incubated for 24, 36 and 36 h, respectively. NCI-H441 cells were treated with Y-27632 (5  $\mu$ M) for 15 min before incubation. For a scratch assay,  $1.5 \times 10^6$  cells were plated in 6-well

plates. After 24 h of incubation, a single linear wound was created with a 200- $\mu$ l pipette tip. An MTT assay was performed with TetraColor One (Seikagaku) according to the manufacturer's instructions.

#### Three-dimensional Matrigel invasion assay and immunostaining

One hundred microlitres of Matrigel (BD Biosciences) was prepared on  $18 \times 18$  mm coverslips in 6-well plates, on which  $2 \times 10^5$  cells were plated and cultured for 48 h, followed by fixation with 3.7% formaldehyde for 30 min and post-fixing with 0.1% Triton X-100 for 30 min at room temperature (RT). Cells were incubated with blocking buffer (1% BSA in PBS) overnight at 4°C and were visualized by staining with Alexa-conjugated phalloidin (Molecular Probes). The coverslips were mounted onto slides using Fluoromount (Diagnostic BioSystems) and analysed using an A1 Rsi confocal microscope (Nikon). The invasion distance was defined as that between the slide glass (top of the Matrigel) and the centre of fluorescence intensity, and measured using MetaMorph (Molecular Devices) software. The extent of collective cell migration was defined as the ratio of collective cells ( $\geq 5$  cells) to total cell number. Data shown represent three independent experiments, with  $>100$  cells counted in each.

#### In-vivo metastasis assay

LNM35 cells ( $1.0 \times 10^7$ ) in 0.1 ml of serum-free RPMI-1640 medium were injected into subcutaneous tissues of the right groin of 6-week-old female SCID mice. Forty days after inoculation, the mice were euthanized, and their lungs and subcutaneous tumours resected, weighed, and fixed with 10% formaldehyde. Lung-metastatic nodules were examined under a dissecting microscope. An experimental metastasis assay following tail vein injection of tumour cells was performed, essentially as described by Shibue and Weinberg (2009). NCI-H441 cells were transfected with either Alexa Fluor 488-conjugated siScr (siScr-AF488) or -siMYBPH #1 (siMYBPH-AF488) as described above, then the transfectants were harvested 48 h later. Cells at  $1.0 \times 10^6$  in 0.1 ml of PBS were injected into tail veins of 6-week-old female SCID mice. Five days after injection, the mice were euthanized, then 6 ml of PBS was injected into the right ventricle for perfusion of the lung microvasculature. The perfused lungs were embedded in OCT (Sakura), sectioned (thickness 10  $\mu$ m) with a Leica CM3050 (Leica Microsystems), and fixed using Fluoromount. Perfusion-resistant cells were determined by direct counting in the sections using an A1 Rsi confocal microscope.

#### Immunostaining

Cells ( $0.5 \times 10^5$ ) were plated on  $18 \times 18$  mm coverslips in 6-well plates and cultured for 12 h. NCI-H441 cells were treated with Y-27632 (5  $\mu$ M) for 15 min before plated. The cells were fixed by incubating with 3.7% formaldehyde for 10 min at RT, followed by post-fixing with 0.1% Triton X-100 for 10 min at RT. Cells were incubated with blocking buffer overnight at 4°C, followed by another incubation with antibodies (diluted in blocking buffer) for 60 min at RT. After treatment with Alexa-conjugated secondary antibodies (Molecular Probes) for 60 min at RT, the coverslips were mounted onto slides using Fluoromount, and analysed using an A1 Rsi confocal microscope.

#### Actin assembly assay

Cells were lysed with buffer containing 1% Triton X-100, 10 mM EGTA, 40 mM NaCl, 10 mM imidazole, and a protease inhibitor cocktail (Roche) at 4°C. The lysates were centrifuged at  $15000 \times g$  for 5 min at 4°C, then the pellets were washed, dissolved in  $1 \times$  SDS sample buffer, and subjected to western blot analysis with an anti-actin antibody. Three independent experiments were performed in triplicate, with similar results obtained.

#### Preparation of recombinant proteins

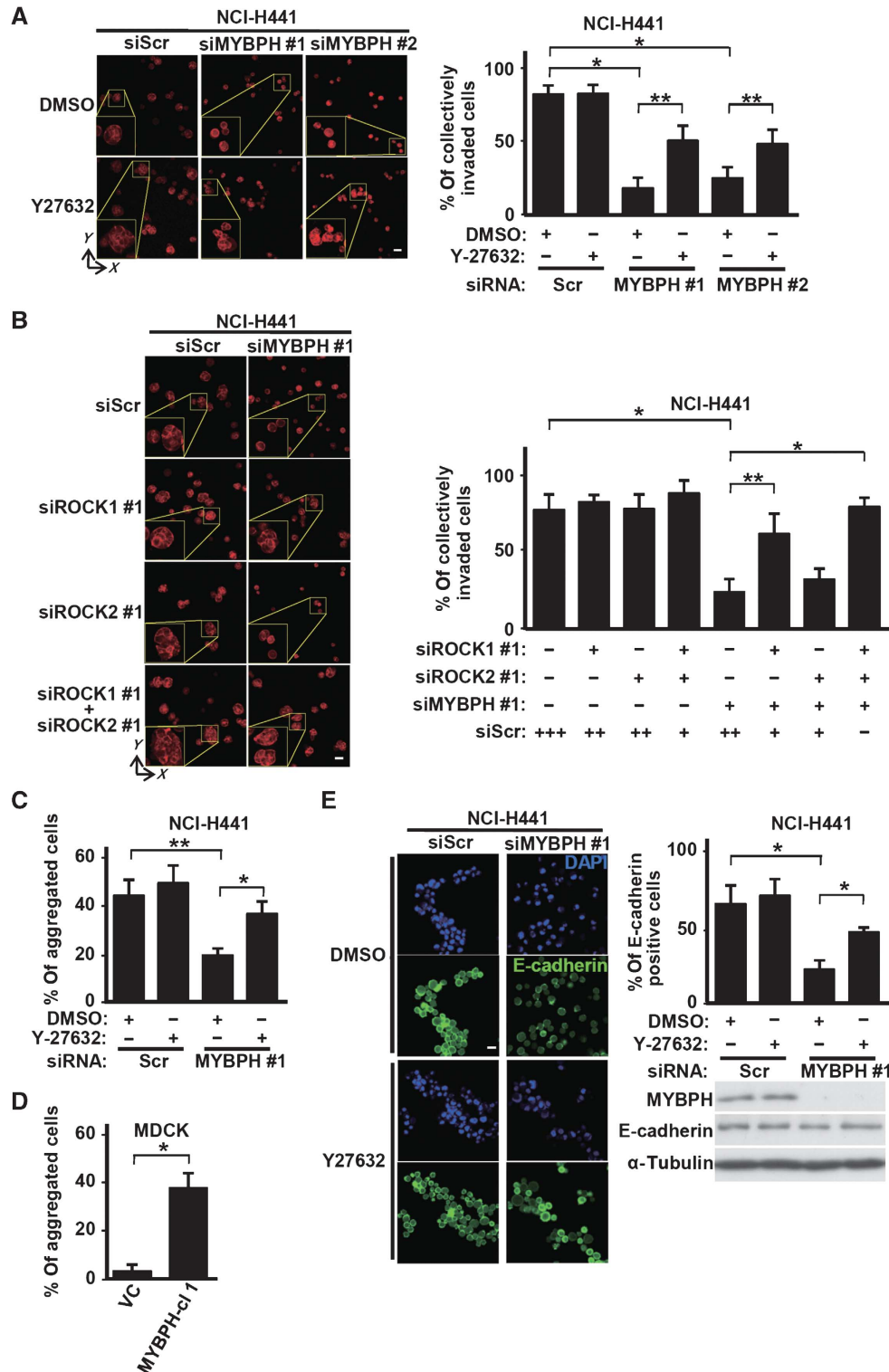
His-tagged MYBPH-wt, - $\Delta 3$ , - $\Delta(2+3)$ , - $\Delta(1+2+3)$ , and - $\Delta 2$  proteins were expressed in Sf9 insect cells using a Gateway system (Invitrogen), according to the manufacturer's instructions. Recombinant His-tagged MYBPH-wt, - $\Delta 3$ , - $\Delta(2+3)$ , - $\Delta(1+2+3)$ , and - $\Delta 2$  proteins were purified using imidazole-affinity chromatography. Recombinant GST-tagged ROCK1 (amino acids 17–535) and GST-tagged ROCK2 (amino acids 5–554) were purchased from Sigma. GST-tagged RLC and GST were from Abnova.

**In-vitro protein-protein binding assay**

Purified His-tagged MYBPH-wt, - $\Delta 3$ , - $\Delta(2+3)$ , - $\Delta(1+2+3)$ , or - $\Delta 2$  was mixed with glutathione beads coated with recombinant GST, GST-tagged RLC, GST-tagged ROCK1, or GST-tagged ROCK2. After repeated washes with a solution containing 20 mM MOPS (pH 7.2), 1 mM dithiothreitol, 5 mM EGTA, 25 mM  $\beta$ -glycerophosphate, 1 mM  $\text{Na}_3\text{VO}_4$ , and 75 mM  $\text{MgCl}_2$ , the bound proteins were eluted and subjected to SDS-PAGE, followed by western blot analysis with anti-ROCK1, anti-ROCK2, anti-RLC, or anti-MYBPH antibodies.

**In-vitro kinase assay**

Purified GST-tagged RLC, GST-tagged ROCK1, and GST-tagged ROCK2 were incubated in phosphorylation buffer (25 mM Tris-HCl (pH 7.5), 5 mM  $\text{MgCl}_2$ , and 0.5 mM ATP) with or without purified His-tagged MYBPH at a final protein concentration of 0.1  $\mu\text{M}$  for 1 h at 37°C. The reactions were analysed by SDS-PAGE, followed by western blot analysis with anti-phospho-RLC antibodies. For detection of phosphorylations, we used an *in-vitro* kinase assay, in which those proteins were incubated in kinase buffer containing 100  $\mu\text{M}$  [ $\gamma$ - $^{32}\text{P}$ ]ATP (2  $\mu\text{Ci}$ ), then resolved by SDS-



PAGE and stained with CBB reagents. Radiolabelled phosphoprotein bands were visualized by autoradiography of a dried gel.

**Cell aggregation assay**

Cells ( $1 \times 10^6$ ) were suspended in RPMI or DMEM medium supplemented with 10% FBS in 12-well plates pre-coated with 2% BSA (Roche), then cultured with horizontal rotation (75–100 r.p.m.) at 37°C for 30 min. Aggregation was fixed by adding 2% glutaraldehyde (Nacalai Tesque). The extent of aggregation ( $\geq 5$  cells) was defined as the ratio of total particle number to initial cell number. Cells were then attached onto a slide glass using a CYTOSPIN device (2000 r.p.m., 5 min) followed by immunostaining,

or were dissolved in  $1 \times$  SDS sample buffer, then subjected to western blot analysis. Cells with intense staining on the cell surface, as shown by MetaMorph software finding, were considered to be E-cadherin positive. Data shown represent three independent experiments, with  $>100$  cells counted in each.

**Statistical analysis**

Statistical analyses of data presented in Figures 2B and 4F were performed using Fisher's exact test. For the other experiments, significance levels were determined by a *t*-test. All statistical analyses are performed in a two-sided manner.

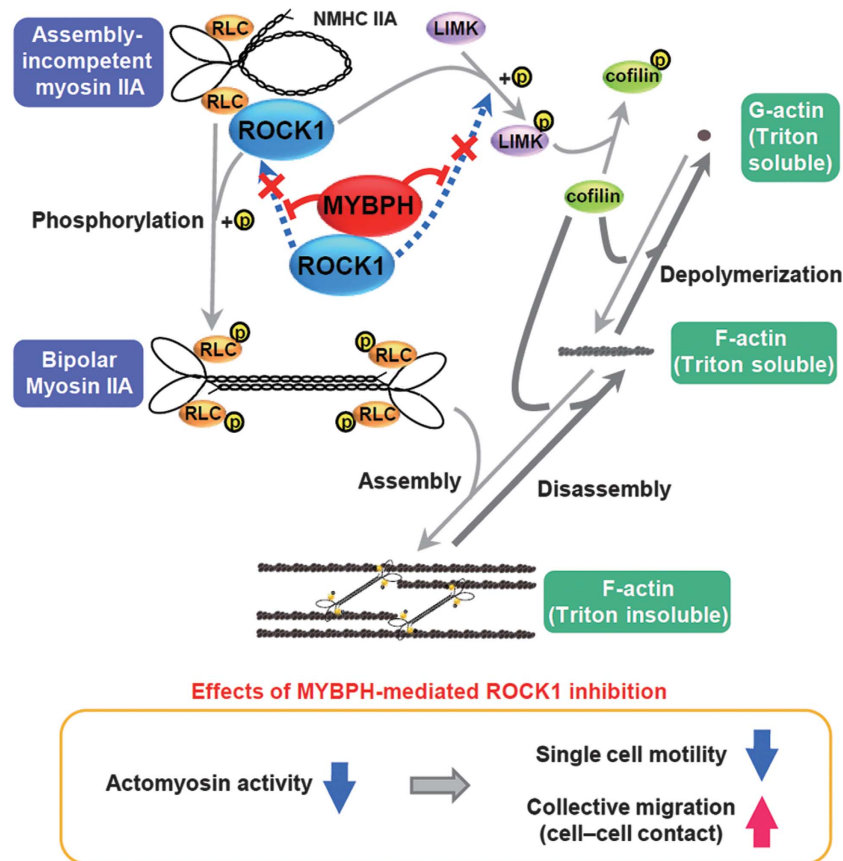


**Figure 9** Schematic diagram demonstrating how MYBPH affects actomyosin organization through inhibition of ROCK1. RLC phosphorylation-mediated bipolar NM IIA formation, a prerequisite for actomyosin assembly, is disturbed by MYBPH via direct interaction with and negative regulation of ROCK1, which also leads to inhibition of the LIMK-cofilin pathway. Consequently, MYBPH inhibits ROCK1-driven actomyosin organization, which in turn reduces single cell motility and promotes collective cell migration.

**Figure 8** MYBPH knockdown reduces cell-cell contact and collective cell migration. (A) Three-dimensional Matrigel invasion assay findings showing decreased collective cell migration by MYBPH knockdown and significant reversion by simultaneous Y-27632 treatment in NCI-H441 cells. Cells were visualized by actin staining (red). White bars indicate 50  $\mu$ m. The proportions of cells with collective invasion were evaluated as in Figure 3D. Data shown represent three independent experiments. Bars, mean  $\pm$  s.d.; \**P* < 0.01. (B) Three-dimensional Matrigel invasion assay findings showing decreased collective cell migration by MYBPH knockdown and significant reversion by simultaneous siROCK1 treatment in NCI-H441 cells. Cells were visualized by actin staining (red). White bars indicate 50  $\mu$ m. The proportions of cells with collective invasion were evaluated as in Figure 3D. Data shown represent three independent experiments. Bars, mean  $\pm$  s.d.; \**P* < 0.01; \*\**P* < 0.05. siRNA concentrations: +, 40 nM; ++, 80 nM; +++, 120 nM. (C) Cell aggregation assay findings showing that MYBPH knockdown decreased formation of cell aggregates and significant reversion by simultaneous Y-27632 treatment in NCI-H441 cells. The proportions of aggregated cells were evaluated as described in Materials and methods. Data shown represent three independent experiments. Bars, mean  $\pm$  s.d.; \**P* < 0.05; \*\**P* < 0.01. (D) Cell aggregation assay findings showing increased numbers of cell aggregates in stable MYBPH transfectants of MDCK cells. Data shown represent three independent experiments. Bars, mean  $\pm$  s.d.; \**P* < 0.01. (E) Immunofluorescent staining of E-cadherin in NCI-H441 cells subjected to cell aggregation assay. Cells were stained with anti-E-cadherin antibody (green) and DAPI (blue), which revealed decreased cell surface E-cadherin expression in NCI-H441 cells knocked down for MYBPH. Note that cell aggregation was also decreased by siMYBPH treatment and these phenotypic changes were significantly reverted when the cells were simultaneously treated with Y-27632. Western blot analysis findings showed negligible changes in total amounts of E-cadherin. Bar indicates 10  $\mu$ m. Proportions of E-cadherin-positive cells were evaluated as described in Materials and methods. Data shown represent three independent experiments. Bars, mean  $\pm$  s.d.; \**P* < 0.01. Figure source data can be found with the Supplementary data.

### Supplementary data

Supplementary data are available at The EMBO Journal Online (<http://www.embojournal.org>).

## Acknowledgements

We would like to thank Takeo Kawahara for the technical assistance, and Takeshi Senga and Hirotaka Osada for the helpful advice and discussion. This work was supported in part by Grants-in-Aid for Scientific Research on Innovative Areas and Scientific Research on Priority Areas from the Ministry of Education, Culture, Sports, Science and Technology (MEXT) of Japan; Grants-in-Aid for Scientific Research (A) and Young Scientists (B) from the Japan

Society for the Promotion of Science (JSPS); and a Grant-in-Aid for Third-Term Comprehensive Strategy for Cancer Control from the Ministry of Health, Labour and Welfare of Japan. YH was supported by a JSPS Research Fellowship.

**Author Contributions:** YH, TY, and TT designed research; YH, TY, EM, KiY, YS, MH, and MS performed research; YH, TY, EM, KiY, CA, ST, SK, KoY, MS, and TT analysed data; and YH, KiY, MS, and TT wrote the manuscript. All authors discussed the results and commented on the manuscript.

## Conflict of interest

The authors declare that they have no conflict of interest.

## References

- Amano M, Nakayama M, Kaibuchi K (2010) Rho-kinase/ROCK: a key regulator of the cytoskeleton and cell polarity. *Cytoskeleton (Hoboken)* **67**: 545–554
- Anagnostou VK, Syrigos KN, Bepler G, Homer RJ, Rimm DL (2009) Thyroid transcription factor 1 is an independent prognostic factor for patients with stage I lung adenocarcinoma. *J Clin Oncol* **27**: 271–278
- Betapudi V, Licate LS, Egelhoff TT (2006) Distinct roles of non-muscle myosin II isoforms in the regulation of MDA-MB-231 breast cancer cell spreading and migration. *Cancer Res* **66**: 4725–4733
- Bonne G, Carrier L, Bercovici J, Cruaud C, Richard P, Hainque B, Gautel M, Labeit S, James M, Beckmann J, Weissenbach J, Vosberg HP, Fiszman M, Komajda M, Schwartz K (1995) Cardiac myosin binding protein-C gene splice acceptor site mutation is associated with familial hypertrophic cardiomyopathy. *Nat Genet* **11**: 438–440
- Chen CY, Schwartz RJ (1995) Identification of novel DNA binding targets and regulatory domains of a murine tinman homeodomain factor, *nkx-2.5*. *J Biol Chem* **270**: 15628–15633
- Christiansen JJ, Rajasekaran AK (2006) Reassessing epithelial to mesenchymal transition as a prerequisite for carcinoma invasion and metastasis. *Cancer Res* **66**: 8319–8326
- Conti MA, Adelstein RS (2008) Nonmuscle myosin II moves in new directions. *J Cell Sci* **121**: 11–18
- Etienne-Manneville S, Hall A (2002) Rho GTPases in cell biology. *Nature* **420**: 629–635
- Friedl P, Gilmour D (2009) Collective cell migration in morphogenesis, regeneration and cancer. *Nat Rev Mol Cell Biol* **10**: 445–457
- Friedl P, Wolf K (2003) Tumour-cell invasion and migration: diversity and escape mechanisms. *Nat Rev Cancer* **3**: 362–374
- Friedl P, Wolf K (2010) Plasticity of cell migration: a multiscale tuning model. *J Cell Biol* **188**: 11–19
- Hall A (2009) The cytoskeleton and cancer. *Cancer Metastasis Rev* **28**: 5–14
- Hidalgo-Carcedo C, Hooper S, Chaudhry SI, Williamson P, Harrington K, Leitinger B, Sahai E (2011) Collective cell migration requires suppression of actomyosin at cell-cell contacts mediated by DDR1 and the cell polarity regulators Par3 and Par6. *Nat Cell Biol* **13**: 49–58
- Huang Y, Arora P, McCulloch CA, Vogel WF (2009) The collagen receptor DDR1 regulates cell spreading and motility by associating with myosin IIA. *J Cell Sci* **122**: 1637–1646
- Itoh K, Yoshioka K, Akedo H, Uehata M, Ishizaki T, Narumiya S (1999) An essential part for Rho-associated kinase in the transcellular invasion of tumor cells. *Nat Med* **5**: 221–225
- Kendall J, Liu Q, Bakleh A, Krasnitz A, Nguyen KC, Lakshmi B, Gerald WL, Powers S, Mu D (2007) Oncogenic cooperation and coamplification of developmental transcription factor genes in lung cancer. *Proc Natl Acad Sci USA* **104**: 16663–16668
- Kimura S, Hara Y, Pineau T, Fernandez-Salguero P, Fox CH, Ward JM, Gonzalez FJ (1996) The T/ebp null mouse: thyroid-specific enhancer-binding protein is essential for the organogenesis of the thyroid, lung, ventral forebrain, and pituitary. *Genes Dev* **10**: 60–69
- Kozaki K, Miyaiishi O, Tsukamoto T, Tatematsu Y, Hida T, Takahashi T (2000) Establishment and characterization of a human lung cancer cell line NCI-H460-LNM35 with consistent lymphogenous metastasis via both subcutaneous and orthotopic propagation. *Cancer Res* **60**: 2535–2540
- Kwei KA, Kim YH, Girard L, Kao J, Pacyna-Gengelbach M, Salari K, Lee J, Choi YL, Sato M, Wang P, Hernandez-Boussard T, Gazdar AF, Petersen I, Minna JD, Pollack JR (2008) Genomic profiling identifies TITF1 as a lineage-specific oncogene amplified in lung cancer. *Oncogene* **27**: 3635–3640
- Lauffenburger DA, Horwitz AF (1996) Cell migration: a physically integrated molecular process. *Cell* **84**: 359–369
- Li J, Gao E, Seidner SR, Mendelson CR (1998) Differential regulation of baboon SP-A1 and SP-A2 genes: structural and functional analysis of 5'-flanking DNA. *Am J Physiol* **275**: L1078–L1088
- Maekawa M, Ishizaki T, Boku S, Watanabe N, Fujita A, Iwamatsu A, Obinata T, Ohashi K, Mizuno K, Narumiya S (1999) Signaling from Rho to the actin cytoskeleton through protein kinases ROCK and LIM-kinase. *Science* **285**: 895–898
- Masuda A, Kondo M, Saito T, Yatabe Y, Kobayashi T, Okamoto M, Suyama M, Takahashi T (1997) Establishment of human peripheral lung epithelial cell lines (HPL1) retaining differentiated characteristics and responsiveness to epidermal growth factor, hepatocyte growth factor, and transforming growth factor beta1. *Cancer Res* **57**: 4898–4904
- Matsumura F (2005) Regulation of myosin II during cytokinesis in higher eukaryotes. *Trends Cell Biol* **15**: 371–377
- Medjkane S, Perez-Sanchez C, Gaggioli C, Sahai E, Treisman R (2009) Myocardin-related transcription factors and SRF are required for cytoskeletal dynamics and experimental metastasis. *Nat Cell Biol* **11**: 257–268
- Pogach MS, Cao Y, Millien G, Ramirez MI, Williams MC (2007) Key developmental regulators change during hyperoxia-induced injury and recovery in adult mouse lung. *J Cell Biochem* **100**: 1415–1429
- Richard P, Charron P, Carrier L, Ledeuil C, Cheav T, Pichereau C, Benaïche A, Isnard R, Dubourg O, Burbano M, Gueffet JP, Millaire A, Desnos M, Schwartz K, Hainque B, Komajda M (2003) Hypertrophic cardiomyopathy: distribution of disease genes, spectrum of mutations, and implications for a molecular diagnosis strategy. *Circulation* **107**: 2227–2232
- Riento K, Guasch RM, Garg R, Jin B, Ridley AJ (2003) RhoE binds to ROCK I and inhibits downstream signaling. *Mol Cell Biol* **23**: 4219–4229
- Riento K, Ridley AJ (2003) Rocks: multifunctional kinases in cell behaviour. *Nat Rev Mol Cell Biol* **4**: 446–456
- Sahai E, Marshall CJ (2002) ROCK and Dia have opposing effects on adherens junctions downstream of Rho. *Nat Cell Biol* **4**: 408–415
- Sahai E, Marshall CJ (2003) Differing modes of tumour cell invasion have distinct requirements for Rho/ROCK signalling and extracellular proteolysis. *Nat Cell Biol* **5**: 711–719
- Shibue T, Weinberg RA (2009) Integrin beta1-focal adhesion kinase signaling directs the proliferation of metastatic cancer cells disseminated in the lungs. *Proc Natl Acad Sci USA* **106**: 10290–10295
- Takeuchi T, Tomida S, Yatabe Y, Kosaka T, Osada H, Yanagisawa K, Mitsudomi T, Takahashi T (2006) Expression profile-defined classification of lung adenocarcinoma shows close relationship



- with underlying major genetic changes and clinicopathologic behaviors. *J Clin Oncol* **24**: 1679–1688
- Tanaka H, Yanagisawa K, Shinjo K, Taguchi A, Maeno K, Tomida S, Shimada Y, Osada H, Kosaka T, Matsubara H, Mitsudomi T, Sekido Y, Tanimoto M, Yatabe Y, Takahashi T (2007) Lineage-specific dependency of lung adenocarcinomas on the lung development regulator TTF-1. *Cancer Res* **67**: 6007–6011
- Tomida S, Takeuchi T, Shimada Y, Arima C, Matsuo K, Mitsudomi T, Yatabe Y, Takahashi T (2009) Relapse-related molecular signature in lung adenocarcinomas identifies patients with dismal prognosis. *J Clin Oncol* **27**: 2793–2799
- Vicente-Manzanares M, Ma X, Adelstein RS, Horwitz AR (2009) Non-muscle myosin II takes centre stage in cell adhesion and migration. *Nat Rev Mol Cell Biol* **10**: 778–790
- Watkins H, Conner D, Thierfelder L, Jarcho JA, MacRae C, McKenna WJ, Maron BJ, Seidman JG, Seidman CE (1995) Mutations in the cardiac myosin binding protein-C gene on chromosome 11 cause familial hypertrophic cardiomyopathy. *Nat Genet* **11**: 434–437
- Watts RG, Howard TH (1992) Evidence for a gelsolin-rich, labile F-actin pool in human polymorphonuclear leukocytes. *Cell Motil Cytoskeleton* **21**: 25–37
- Weir BA, Woo MS, Getz G, Perner S, Ding L, Beroukhi R, Lin WM, Province MA, Kraja A, Johnson LA, Shah K, Sato M, Thomas RK, Barletta JA, Borecki IB, Broderick S, Chang AC, Chiang DY, Chirieac LR, Cho J *et al* (2007) Characterizing the cancer genome in lung adenocarcinoma. *Nature* **450**: 893–898
- Welikson RE, Fischman DA (2002) The C-terminal IgI domains of myosin-binding proteins C and H (MyBP-C and MyBP-H) are both necessary and sufficient for the intracellular crosslinking of sarcomeric myosin in transfected non-muscle cells. *J Cell Sci* **115**: 3517–3526
- White CW, Greene KE, Allen CB, Shannon JM (2001) Elevated expression of surfactant proteins in newborn rats during adaptation to hyperoxia. *Am J Respir Cell Mol Biol* **25**: 51–59
- Wilkinson S, Paterson HF, Marshall CJ (2005) Cdc42-MRCK and Rho-ROCK signalling cooperate in myosin phosphorylation and cell invasion. *Nat Cell Biol* **7**: 255–261
- Winslow MM, Dayton TL, Verhaak RG, Kim-Kiselak C, Snyder EL, Feldser DM, Hubbard DD, DuPage MJ, Whittaker CA, Hoersch S, Yoon S, Crowley D, Bronson RT, Chiang DY, Meyerson M, Jacks T (2011) Suppression of lung adenocarcinoma progression by Nkx2-1. *Nature* **473**: 101–104
- Wong CC, Wong CM, Ko FC, Chan LK, Ching YP, Yam JW, Ng IO (2008) Deleted in liver cancer 1 (DLC1) negatively regulates Rho/ROCK/MLC pathway in hepatocellular carcinoma. *PLoS One* **3**: e2779
- Yamamoto K (1988) Effect of H-protein on the formation of myosin filaments and light meromyosin paracrystals. *J Biochem* **103**: 274–280
- Yatabe Y, Mitsudomi T, Takahashi T (2002) TTF-1 expression in pulmonary adenocarcinomas. *Am J Surg Pathol* **26**: 767–773
- Yoneda A, Multhaupt HA, Couchman JR (2005) The Rho kinases I and II regulate different aspects of myosin II activity. *J Cell Biol* **170**: 443–453
- Yoshioka K, Foletta V, Bernard O, Itoh K (2003) A role for LIM kinase in cancer invasion. *Proc Natl Acad Sci USA* **100**: 7247–7252